Grid Connected PV/Wind System Control Techniques for under Distortions and Unbalance Fault Conditions

Ravi Bukya[1], Charan Singh Banothu[2], Attuluri Rakada Vijay Babu[3], B. Mangu[4]

[1]Dept. of EEE, (Malla Reddy College of Engineering and Technology), Associate Professor, Maisamma Guda, Secundrabad, Telangana,India, Email:braviou1@gmail.com
[2]Dept. of EEE, (VFSTR Deemed to be University, Gunturu) ADE TG Transco, Secundrabad, Tealnagana, India, Email: charansingh.banothu@gmail.com
[3]Dept. of EEE (VFSTR Deemed to be University, Gunturu), Professor, Gunturu, Andhra Pradesh, India, Email: arvb_eee@vignan.ac.in
[4]Dept. of EEE (Osmania University, Hyderabad), Professor Hyderabad, Telangana, India, Email: bmanguou@gmail.com

ABSTRACT
This study emphasizes the importance of developing algorithms for controlling and synchronizing voltage source inverters (VSIs) used as power conditioners in grid-connected PV systems for renewable energy. The main goal is to develop and improve algorithms that ensure grid inverters work properly, especially during utility grid disruptions including voltage imbalances, frequency fluctuations, and harmonic distortions. The goal is to demonstrate collaboration clearly. Power quality standards are crucial. The control method uses a proportional resonant (PR) controller with harmonic compensation to improve system efficiency during disturbances. The synchronizations algorithm uses a dual second-order general-purpose integrator frequency-locked loop (DSOGI-FLL). MATLAB/SIMULINK from Math Works, Inc. simulates both techniques to verify their usefulness. This research improves our knowledge and technology of grid-connected solar systems. It provides a complete solution to ensure these systems work optimally and meet power quality criteria during grid outages. This study uses incremental conductance maximum power point tracking (MPPT) and perturb and observe (P&O) methods to overcome restrictions in grid-connected photovoltaic (PV) systems. Fuzzy logic regulators ensure rapid dynamic response, minimize grid current variations, and stabilize voltages within the constant current band, addressing these issues. The proposed approach was thoroughly analyzed, including MATLAB simulations and mathematical calculations. Comparative analysis shows good dynamic performance and improved grid power utilization, proving the utility of the suggested control approach.

Keywords: Voltage Source Inverter, DSOGI-FLL, perturb and observe, photovoltaic, MPPT-Fuzzy logic.

INTRODUCTION
A distributed generation system (DG) connects multiple renewable energy sources to a three-phase low-voltage system via an inverter. The major network power supply is the inverter[1]. Renewable energy sources work better with this setup. Maximum efficiency requires consistent power factor (PF) alignment between grid voltage and inverter current[2]-[13]. Successful synchronisation requires an algorithm that smoothly coordinates the three-phase grid and renewable energy source[3]-[22]. Novel control approaches connect PV generation to the grid without Phase-Locked Loop (PLL) technology to improve system efficiency [4]-[19]. This method can also replace proportional-integral (PI) control in three-phase networks with abrupt load variations, partial malfunctions, solar radiation frequency and intensity fluctuations, and harmonic distortion[5]-[16]. This replacement improves controller operation. Power control technology is important for grid-connected PV inverters[6]-[18]. Comparatively, proportional resonant controllers eliminate selective noise and have zero steady-state error due to their infinite gain at a specific frequency.[7]-[21].
Nevertheless, PR regulators possess some limitations.
1. Perturbations introduced into the voltage loop have a significant impact on the power quality associated with the network.
 2. Phase-locked loops are crucial for the system.
3.In order to address the aforementioned issues, a novel fuzzy-based controller is introduced in this context.

Solar photovoltaic (PV) sources are popular due to their low maintenance and environmental friendliness. Capital costs can also be reduced by grid-connected photovoltaic (PV) systems, which eliminate energy storage batteries. Solar power system performance and investment efficiency depend on energy production efficiency, quality, and reliability. New, renewable, and limitless energy sources must be added to the power network, such as distributed generation (DG) systems, to reduce the greenhouse effect. Integrating must be done carefully, following laws, operational conditions, and primary energy supply networks.

Temperature and solar irradiation must be considered for a grid-connected photovoltaic (PV) system to work properly. To meet international requirements, inverter power factor (PF) management and power quality must be prioritised. Harmonic regulation requires precise compliance with a 5% total harmonic distortion limit. A bespoke current regulator is essential for three-phase inverter current management. Synchronisation can control power factor (PF). Optimal dynamics in a three-phase network need voltage phase angle regulation.

Key findings of research

According to sources [17]-[31], grid-integrating PV generating systems is difficult. Renewable energy sources are integrated into the electricity system via system-tie inverters. As described in references [18]-[32], the inverter in a PV-connected grid system controls and adjusts PV output phase and magnitude. This regulation uses utility grid input, as stated in sources [19]-[33]. Photovoltaic (PV) generator integration with the electrical grid presents many obstacles.

• Synchronization of PV generator with Grid with proper feedback system .
• With the use of conventional current regulators the performance of the inverters will be Poor.
• MMPT schemes like P&O algorithm introduces ripples into the system
• Reel power injected is less due to the above mentioned issues.
• Interfacing PV generator and utility with the help of Advanced Neuro Fuzzy Inference System(ANFIS) controller to improve the performance.
• Enhanced current control to improve the settling time of PV system.
• To reduce the ripples and peak overshoots in dc voltage.
• To design the renewable EV charging station.

Due to the depletion of conventional energy sources, solar, wind, and geothermal energy are becoming more popular. Many distributed generation (DG) systems using these sustainable energy sources are being designed and connected to the power grid. Wind and solar photovoltaic (PV) systems might generate 20% of electricity by 2030. Our electricity grid will incorporate these systems. This study focuses on a solar-powered distributed generation (DG) system. Solar energy is getting more critical, efficient, ecologically beneficial, and emission-free as solar power producing technology advance.
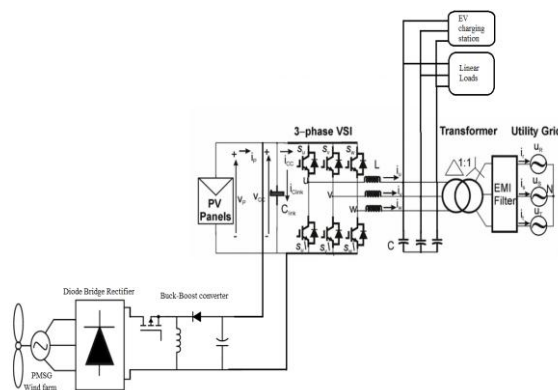

Fig 1. Grid-connected PV system block diagram.

Distributed Generation (DG) systems like synchronous generators emphasise harmonic compensation above active and reactive power[32]. This attention greatly improves control accuracy and system stability[33].

The research paper begins with an overview of the field, topics, and background. Section II divides grid-connected PV systems using PI Controllers into control and power subsystems. A fuzzy logic controller is recommended to address the concerns mentioned above. MPPT Algorithm use in MATLAB Math is covered in Section III. Established approaches such fractional OC voltage, fractional short-circuit current, voltage (current) feedback approach, differentiation, P&O, and INC are implemented. The simplicity and convenience of implementation utilising MATLAB Simulation tools make P&O and INC MPPT algorithms stand out. The theoretical background and computational methods will be examined in detail in this part.

Section IV displays the Grid Connected PV System simulation results, including experimental technique, components, and results. Section V covers simulation and experimental findings analysis and interpretation. This contains data analysis, ramifications discussion, and consideration of figure 1's Grid Connected PV System.

Each segment is organised and deepened by the study project, starting with a contextual component that provides background before exploring the specialised sections.

Performance of Grid-Connected PV Systems Using Traditional PI Controllers

Grid-connected solar systems must efficiently transmit power between the public power grid and the main renewable energy source to work well. The inverter's power factor and grid connection must be precisely managed.

The Perturb and Observe (P&O) method is used as a Maximum Power Point Tracking (MPPT) algorithm in commercial Solar Photovoltaic (SPV) systems due to its simplicity and ease of implementation. Some publications call this the Hill Climbing (HC) algorithm. Two methods are nearly identical, except for the parameter they edit. Perturb and Observe (P&O) modifies the operating voltage, whereas Hill Climbing (HC) perturbs the Pulse Width Modulation (PWM) signal duty cycle. The method constantly modifies the operating point utilizing the derivative of module power as a function of module voltage to obtain the Maximum Power Point (MPP).
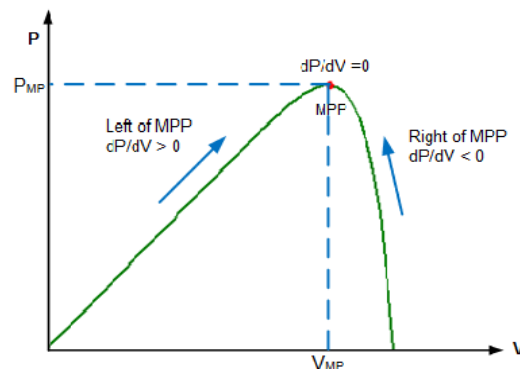

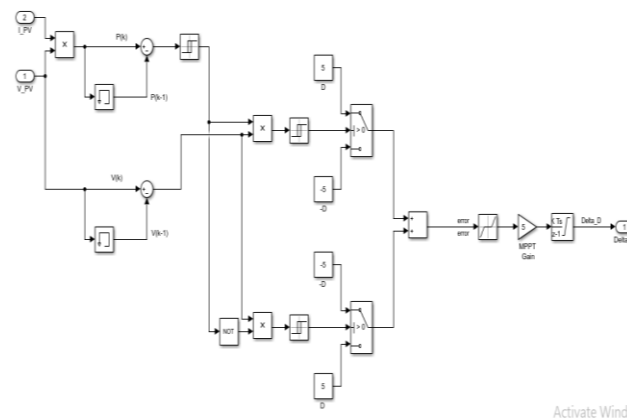**Fig 2.** PV module power-voltage curve

Fig 3. Illustration the Simulink model of P&O Algorithm

The MPPT uses the P&O algorithm because of its simplicity and widespread use. However, the oscillating nature and vulnerability to rapid insolation changes provide challenges. These limits must be addressed to establish a compromise between accuracy and convergence speed to efficiently harvest power from PV modules in varied climates.

Although popular, the P&O MPPT algorithm has major limitations. Even after stabilising, the system oscillates near the MPP, reducing output power. It also struggles to respond to sudden solar radiation changes, which may cause it to miss the Maximum Power Point. The perturbation size is kept small to reduce oscillations. However, this slows convergence, making it take longer to reach the maximum power point. However, increasing disturbance to speed convergence increases power losses. This situation

emphasises the significance of carefully balancing accuracy and convergence speed while constructing algorithms.

Using an LC filter to link the transformer to the inverter's output stabilises voltage. This reduces inverter output variability, improving it. The inverter output current's IGBT rectification ripple frequency produces lesser harmonics due to nonlinear loads. The transformer downstream of the LC or LCL filter separates the grid from the PV array and allows galvanic isolation for maintenance in a grid-tied PV system.
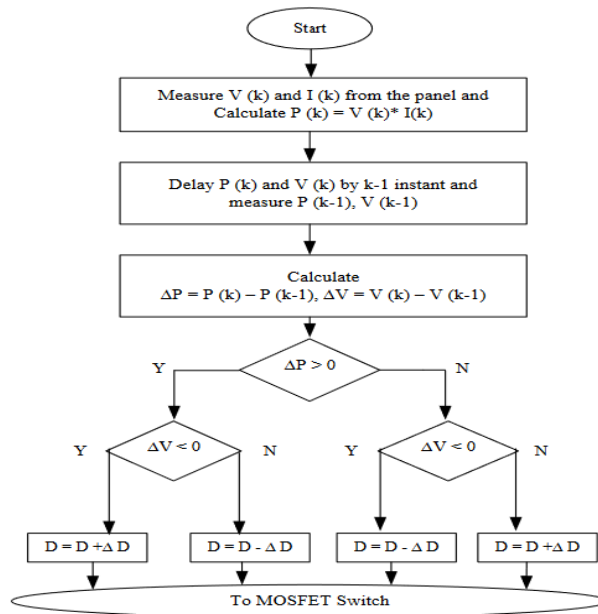

Fig 4. Flow Chart of P&O Method MPPT Algorithm

The SPV systems need efficient active and reactive power management to perform well. MPPT optimises power generation to achieve this goal. MPPT is needed because PV cell efficiency ranges from 12% to 20%. P&O and INC MPPT algorithms differ in tracking speed, complexity, and hardware implementation.

PV panel size in parallel-series arrangement depends on solar system power. Inverters convert DC electricity into AC currents for easy integration with the low-voltage 3-phase utility system. PWM and SVM are essential for effective power conversion and grid integration. Grounding leakage current and solar panel parasitic capacitance plague non-isolated PV inverters. In grid-connected solar systems, harmonic pollution from electromagnetic interference (EMI) must be considered. Diodes and IGBTs cause EMI. EMI filters are essential to reduce this interference. Table 1 shows grid-connected PV system specifications.

Table 1. Grid Connected PV System Parameters

Name of the module	Parameters
Grid	132kV, 50Hz, 2500MVA
PV array	V_{mp}=54.7V, Imp=5.58A, Voc=64.2V, Isc=5.96A, Ns=10, Ns=60, Ppv 97kW.
Wind farm	Pwf=35kW, Vdc=560V, Trated=111Nm, Nrated=3000rpm, Rs=0.05ohms, Ls=0.635mH, Phi=0.192V.s, p=4, J=0.011kgm². Lbb=1mH, Cin=1000uF, PSF MPPT algorithm. fs=5kHz.
Inverter	Cin=10mF, Ron=0.001ohm, Lf=250uH, Cf=70kVAR.
Control	DSOGI-FLL, wn=314.16rad/s, Incremental conductance MPPT, PR- Kp=0.0211, K1=K2=K3=10, w1c=w5c=w7c=10, wo=314.16rad/s, k=1.41, Ts=1usec, fs=5kHz.
Loads	L1=L2=200kW, 100kVAR. Step change at 2sec, EV load 30A.

In Figure 5, photovoltaic (PV) panels in tandem with a wind farm controlled by a PMSG are the input sources. The photovoltaic panels directly connect to the inverter because they create DC voltage. The wind farm's PMSG generates three-phase AC voltages that must be converted to DC by a diode bridge rectifier. A buck-boost unidirectional converter stabilises DC voltage. Six IGBT switches regulate high voltages and currents in the inverter. The LC filter reduces harmonics by converting PWM 3-phase AC signals to 3-phase sine voltages. A 1:1 isolation or step-up transformer transfers surplus PV and wind farm electricity to the grid when needed. These include basic linear loads that change abruptly and an EV charging station with AC-DC converters to power batteries.
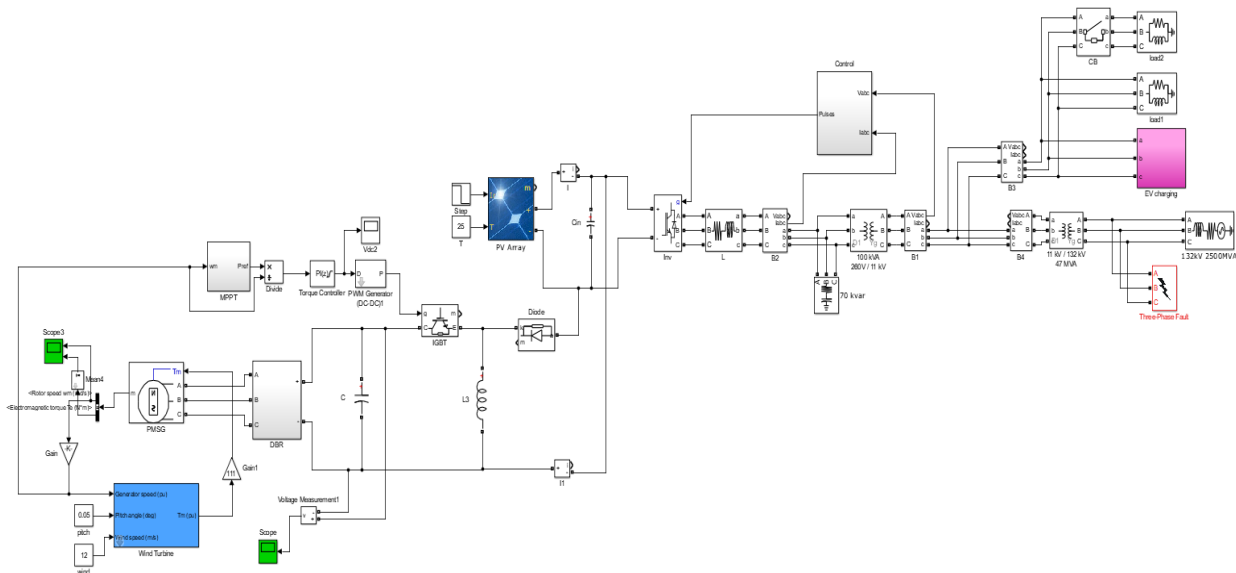

Fig 5. Simulation modeling of the proposed test system with PV and wind farm

A. Power subsystem

The PV panels, an inverter, an LCL filter, and EMI filters comprise the power subsystem power supply. One option uses a two-degree-of-freedom three-wire system with three-phase utility grid and LCL filter. Solar photovoltaic panels generate utility electricity by adjusting to temperature. Parallel-series photovoltaic (PV) panel sizes depend on solar system power needs. The inverter converts DC electricity to AC to fit into the low-voltage 3-phase utility system. This conversion uses diodes and IGBTs. Power switch gate signals are properly managed using PWM and SVM. This optimises power conversion, grid integration, and voltage/current consistency. The PV module feeds the inverter with a capacitor across its output terminals to maintain DC voltage. Direct electricity is converted to alternating current via the inverter.

$$i_p = i_{clink} + i_{cc} \qquad (1.1)$$

$$i_{cc} = S_{12}, i_{12} + S_v . i_v + S_w . i_w \qquad (1.2)$$

$$I_{clink} = C_{link} \frac{d_{vcc}}{d_t} \qquad (1.3)$$

$$P_{pv} = i_p v_p \qquad (1.4)$$

where $i_p v_p$ are PV Panel output current and voltage.

PPV is power available at a given irradiance and cell temperature.

V_{cc} is the dc bus voltage.

i_{clink} is the current through the link capacitor Clink.

and i_{cc} is the current delivered to the 3-phase VSI (which is a function of the line currents iu, iv, iw and the pole states su, sv, sw (1: "on", 0:).

An LC filter stabilises voltage and eliminates ripple when connecting the transformer to the inverter output. The inverter output current IGBT rectification ripple frequency may have lower harmonics due to nonlinear loads. Fix this with an AC inverter LC or LCL filter. Reduce lower harmonic amplitude for network power quality. This is difficult without a harmonic compensator.

After the LC or LCL filter, grid-tied PV systems connect the transformer. This connector provides galvanic grid isolation for the PV array. Low-frequency transformers are less flexible and costlier for inverters. HF transformers are used more in inverters. New circuit boards have coreless magnetic components. Grounding leakage current and solar panel parasitic capacitance affect non-isolated PV inverter power. EMI harmonic pollution affects grid-connected solar installations. An EMI filter on the power grid reduces IGBT and diode EMI.

$$u - u_{AC} = R_i + L\frac{di}{dt} = u_R + u_L \qquad (1.5)$$

Here u, i are the inverter voltage and line currents respectively.

u_{AC} - space vector of supply network voltage of the corresponding instantaneous three-phase variable

L - line inductance
R - copper resistance.

Instantaneous reactive power theory can evaluate power transmission between the three-phase Voltage Source Inverter (VSI) and utility grid. Equations (1.6) and (1.7) calculate instantaneous reactive power (q) and active power (p).

$$p = v_{ac_\alpha} i_a + v_{ac_\beta} i_\beta \qquad (1.6)$$

$$q = v_{ac_\beta} i_\alpha + v_{ac_\alpha} i_\alpha \qquad (1.7)$$

The α,β components of 3-phase voltages and are represented by vacα, vacβ, iα, and iβ.

B. Control Sub System

The MPPT algorithm, synchronisation algorithm, outer voltage PI, and inner current PR regulators are crucial to the control subsystem assembly. A solar system's MPPT algorithm maximises PV panel power, enhancing system efficiency.

i). Synchronization Algorithm

Power factor management requires synchronisation. This method takes into consideration harmonics, voltage imbalances, and frequency changes in order to calculate the most efficient and responsive phase of three-phase utility grid voltages. Malfunctions in sensors can generate secondary harmonics, which need to be recognised. In the conventional dqPLL technique used in the synchronous reference frame, any imbalances in the grid voltage might result in the generation of second-order harmonics in the DC bus voltage.

The challenges are resolved by a PSD block. The Power Spectral Density (PSD) effectively gathers 3-phase utility grid voltages, removing voltage imbalances and harmonic distortions, when employed in conjunction with the dq Phase-Locked Loop (PLL) synchronisation approach.

This article also discusses the identification of phase and frequency voltage fluctuations in three-phase power grids. The method regulates the αβ voltage components (vαβ) in the stationary reference frame of the Frequency-Locked Loop by utilising the Dual Second Order Generalised Integrator (DSOGI). In addition, the SOGI-QSG method produces in-phase and quadrature signals for vαβ. This method employs a pair of Second Order Generalised Integrators (as seen in Figure 6).
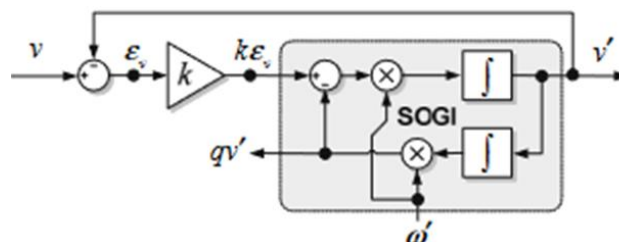

Fig 6. Second Order Generalised Integrator with Quadrature Signal Generation is SOGI-QSG.

$$D(s) = \frac{v'}{v}(s) = \frac{k\omega' s}{s^2 + k\omega' s + \omega'^2} \qquad (1.8)$$

$$Q(s) = \frac{qv'}{v}(s) = \frac{k\omega' s^2}{s^2 + k\omega' s + \omega'^2} \qquad (1.9)$$

The equations for band-pass and low-pass filters require the centre angular frequency of the adaptive filter (ω′) and the gain of the SOGI block (k). Equation 2 shows a constant time delay of 900 between qv' and v,

regardless of ω' and k changes. Equations (1.8) and (1.9) are second-order transfer functions. As shown in table 2, the system's behaviour depends on the complex plane poles' position relative to k.

Table 2. The SOGI-QSG as per the Information Pertaining to "k"

k	SOGI-QSG	Overshoot(%)	Settling Time(ms)	Harmonics rejection of Q(s) (dB)	
				5th	**7th**
1	1	0	28.4	27.73	-33.8
1.28	0.85	1.6	24.5	25.90	31.82
1.416	0.708	4.4	21.8	24.92	30.79
2	0.5	16.4	14.7	-22.24	-27.96

Harmonics are eliminated via band-pass and low-pass filters. Deciding the value of k for a given ω' needs compromise. To optimise performance, the bandwidth for rejecting harmonics, system settling time, and dynamic response overshoot must be balanced.

ii). Frequency Locked Loop (FLL)

FIGURE 7 shows how frequency locked loops (FLLs) accurately monitor input signal v frequency ω. The output frequency of the input signal v is represented by ω', which may be measured without trigonometric functions. This makes it suitable for standard microcontrollers. To enhance the algorithm's dynamic reactivity, use the correct nominal frequency ωc in this block.
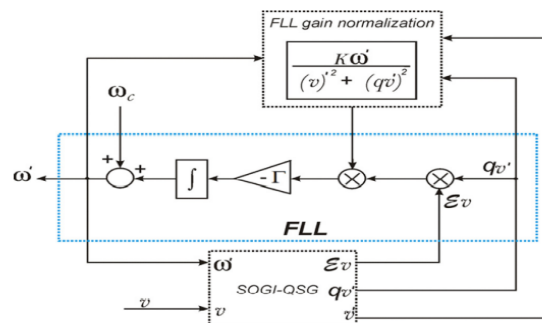

Fig 7. Block diagram of GAIN Normalization for Frequency-Locked Loop

The FLL gain is normalised to eliminate its dependence on utility grid voltage amplitude and SOGI-QSG block gain k. FLL can be simplified as a linearized first-order system in steady-state. This system uses the SOGI-QSG block's nominal output points and one integrator. In equations (1.10), the settling time ts(FLL) can be estimated using 5τ, where τ is $1/\Gamma$ and represents the first-order system's time constant.

$$ts\left(FLL\right) \square \frac{5}{\Gamma} \qquad (1.10)$$

According to the given information, here is the revised content in the desired writing style:

"It is important to mention that the 'u' measurement represents the feedback of the 'qv' signal from the SOGI-QSG block." The characteristics of the low-pass filter in the transfer function Q(s) (as stated in Equation 17) may be responsible for the presence of harmonic contamination in this signal. Figure 8 provides further clarity by presenting the extended structure of the DSOGI-FLL, which includes the analysis of 3-phase systems."
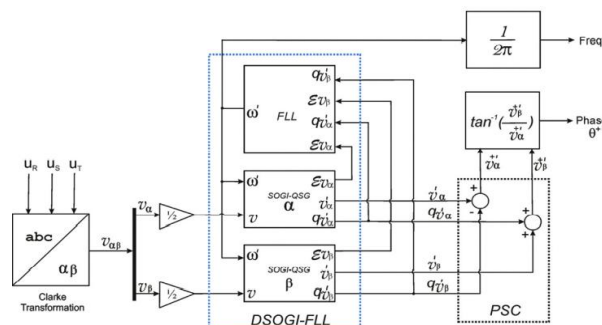

Fig 8. Block diagram of DSOGI-FLL Synchronisation Algorithm

Two SOGIQSG blocks generate in-quadrature signals by transforming input 3-phase voltages into αβ voltage components (vαβ) using the Clarke transformation. To represent the immediate positive sequence component (v+αβ) of the voltage vector vαβ, use equations (1.11) and (1.12).

$$v^+{}_{\alpha\beta} = \frac{1}{2}\begin{pmatrix} 1 & q \\ q & 1 \end{pmatrix} v_{\alpha\beta} \qquad\qquad (1.11)$$

Where A phase-shift operator is represented by $q = e^{-j\frac{\pi}{2}}$.

The in-quadrature waveform component must be obtained using a Positive Sequence Calculator (PSC). Follow equations (1.12) to construct and use a customised calculator to process in-quadrature output signals and identify the positive sequence of the input 3-phase unbalanced voltages. The phase angle for the positive sequence component of three-phase utility grid voltages is computed as follows.

$$\theta^+{}' = \tan^{-1}\left(\frac{v+'{}_{\beta}}{v+'{}_{\alpha}}\right) \qquad\qquad (1.12)$$

DSOGI-FLL structure performance is evaluated by observing the temporal evolution of the observed frequency in simulations. Dynamic responsiveness of three-phase utility grid voltages is assessed using varied gains (Γ) and frequency adjustments of 50-60 Hz. FLL accomplishes extended settling time by using a small Γ value (50-70). Setting Γ to 100 results in a settling time of around 2.5 cycles, which differs from table 3.

Table 3. Relationship between the GAIN (Γ) and Settling Time (Ts)

Γ	50	70	100
ts(FLL) (ms)	100	70	50

Table 3 presents the correlation between the gain Γ and the corresponding settling time ts(FLL) when a step of frequency ranging from 50 Hz to 60 Hz is applied to the utility grid frequency.

iii). Cascade Control

This hierarchical control system features external voltage and internal current regulators. Outer loop regulator compares DC bus voltage to MPPT reference for consistency. It assures PV-grid power distribution uniformity. An outer loop of the inverter system creates the reference d-component of the 3-phase currents (id) in the synchronous reference frame (dq) utilising proportional-integral (PI) regulators. Reference q-component controls open-loop inverter-grid power factor. To improve system stability, overshoot, and settling time, Ki and Kp are carefully selected PI regulator constants. According to [21, 48], the phase margin is 63.5.

Due to integral components, traditional proportional-integral (PI) regulators reduce steady-state dc signal inaccuracies. Zero steady-state error in sinusoidal signal processing requires PR regulators. Generalised integrators (GIs) can conceptualise PR regulators' resonance [25]. Three-wire 3-phase unbalanced systems with two PR controllers track positive- and negative-sequence 3-phase sinusoidal references (figure 9). The internal model suggests that controllers are robust to three-phase sinusoidal disturbances due to their transfer functions, which have complex conjugate poles at the fundamental resonance angular frequency (ω0 and - ω0) in the complex plane.
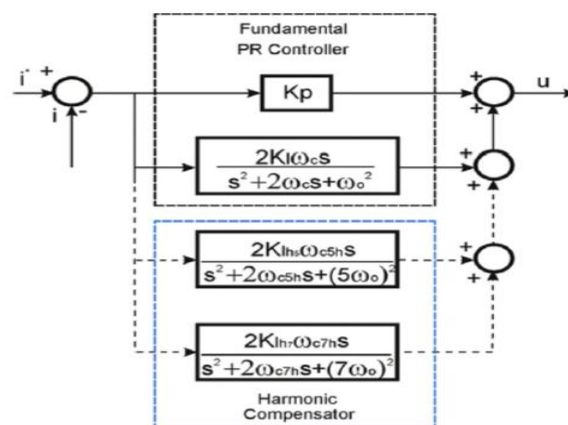

Fig 9. Proportional Resonant Control with Harmonic Compensator Strucure

The inverse Park Transformation is utilized to transform the variables i_d^* and i_q^*, resulting in the reference currents that are sinusoidal i_α^* and i_β^*. The Clarke transformation (abc to αβ) is then applied to the line currents of the three phases, assessing the sinusoidal αβ components of them. These components are then compared with i_α^* and i_β^* Two Proportional Resonant (PR) controllers in the Stationary Reference Frame (αβ) receive the resulting errors as input. The outputs of the controllers represent the average reference sinusoidal inverter voltage($u_{\alpha\beta}^*$).In the three-phase inverter, the Space Vector Modulation (SVM) block closes the inner current loop to determine power pole state. In steady-state settings, this synchronises inverter line currents with utility grid voltages, eliminating inaccuracy. It also dampens utility grid voltage fluctuations, eliminating the requirement for feed-forward open-loop control. The proportional gain Kp, which is tuned similarly to how a PI controller is tuned, alters the bandwidth, phase, and gain margin behaviour of the system. Since the steady-state error depends on the integral gain KI, its value needs to be chosen to be suitably large while staying within the bounds of stability. Additionally, ωc should be empirically set to a range of 5 – 15 rad/s, as this has shown good results as follows eq'ns (1.13) and (1.14).

$$G_{PR} = K_p + \frac{2K_1 \omega_c S}{S^2 + 2\omega_c S + \omega_0^2} \qquad (1.13)$$

Additionally to the PR controller, the Harmonic Compensator (HC) structure utilises numerous cascaded generalised integrators (GI) that resonate at unique low-order harmonic angular frequencies. This structure reduces low-frequency harmonic disturbances in 3-phase utility grid voltages, according internal model theory. Providing acceptable utility power quality takes little computing. The Harmonic Compensator (HC) transfer function is (3.14), where 'h' is the harmonic to correct. Changing Ki and ωc parameters is like modifying the non-ideal PR controller.

$$G_h(s) = \sum_{h=5,7} \frac{2K_{h1} \omega_{hc} S}{S^2 + 2\omega_{ch} S + h\omega_0 2} \qquad (1.14)$$

Figure 9 illustrates the generic Proportional Resonant (PR) controller and the Harmonic Compensator (HC) structure for the 5th and 7th harmonics, extendable to other low-frequency perturbations.

Implementation Of Conventional Mppt Algorithms For Solar Photovoltaic System

Traditional MPPT methods examine the SPV module's voltage, current, or both to discover the Maximum Power Point. Commercial Solar Photovoltaic (SPV) applications employ the Perturb & Observe (P&O) MPPT Algorithm because to its simplicity and ease of implementation. P&O and HC, often known as the Hill Climbing algorithm, are essentially identical save for the parameter adjustment. Perturb and Observe (P&O) changes the operating voltage, whereas Hill Climbing (HC) changes the PWM duty cycle. Duty cycle changes effect PV module output voltage reciprocally.

Hill climbing involves tweaking duty cycle (D) to test module power. If the modification increases power, the direction is maintained; otherwise, it changes. To obtain the Maximum Power Point, the algorithm constantly updates the operating point based on module power and voltage (dP/dV). The method raises voltage to reach the MPP when dP/dV is larger than zero. The software lowers voltage to reach MPP when dP/dV is less than zero.

The P&O MPPT algorithm has drawbacks. Power losses occur when the system oscillates about the maximum power point (MPP) after stabilising. Solar radiation fluctuations can mistrack the Maximum Power Point (MPP) and degrade performance. To reduce oscillations, minimising disturbance magnitude reduces convergence rate, making it take longer to reach the maximum power point (MPP). However, increasing disturbance to hasten convergence increases power losses. We need careful algorithm development to balance precision and solution speed.
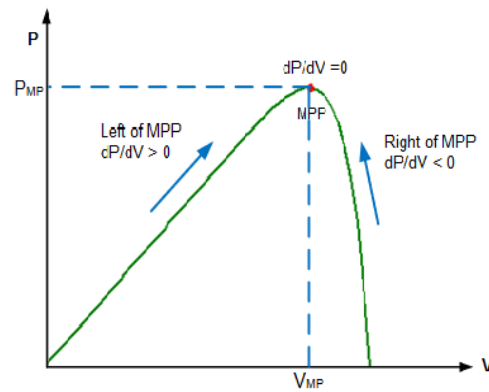
Fig 10. Power-Voltage (P-V) Characteristic Curve of a PV Module

Figure 11, Simulink model of P&O MPPT method. Current and module voltage are inputs; duty cycle is output. Figure 10 shows the algorithm flow. Simulink and flow charts explain algorithm structure. To summarise, P&O is a popular and simple MPPT algorithm, but its oscillation and susceptibility to rapid insolation fluctuations present issues. These constraints must be addressed to balance precision and system solution speed. This optimises PV module power extraction in different climates.
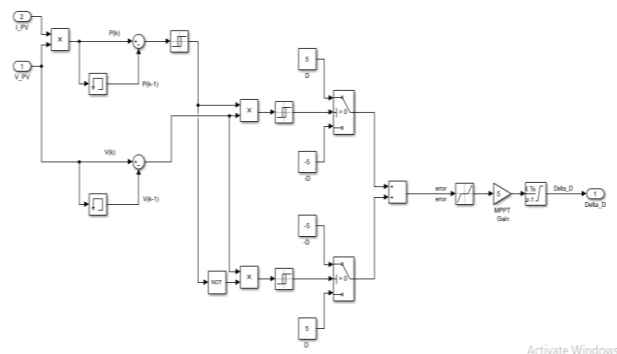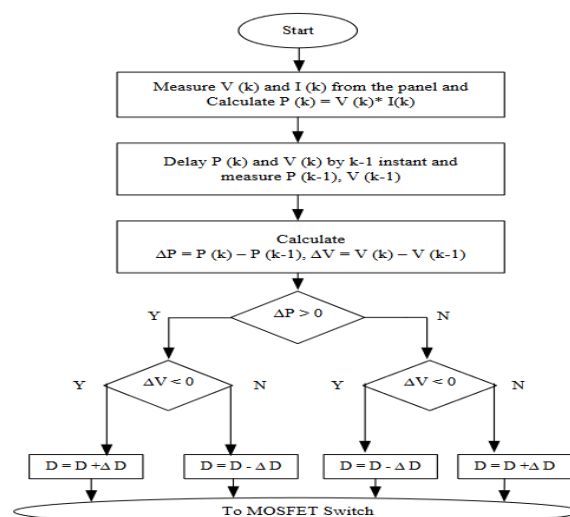

Fig 11. Simulink Model of P&O Algorithm

Fig 12. Flow Chart Illustrating the P&O and MPPT Algorithm

FIGURE 13, The Incremental Conductance (INC) approach is chosen over the Perturb and Observe (P&O) method because to its better performance. It improves efficacy by monitoring quickly changing irradiation with efficiency. This approach assumes that the Maximum Power Point (MPP) is reached when the Power-Voltage (P-V) curve slope is zero, as illustrated in Figures 11 and 12..
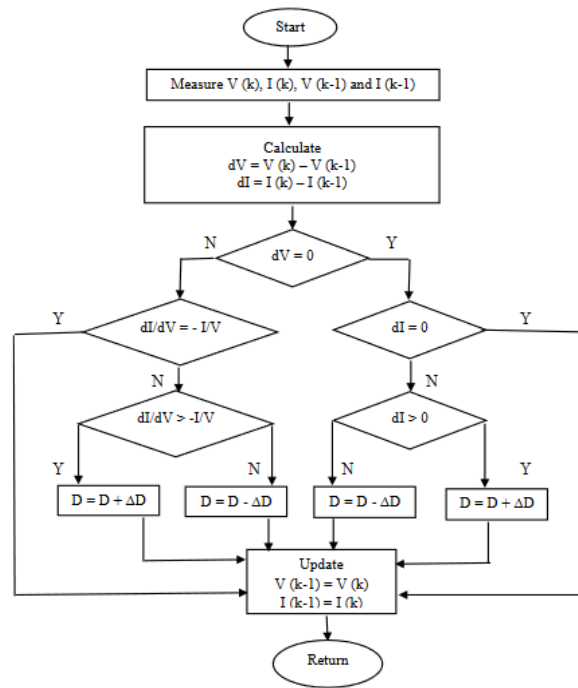
Fig 13. Diagram illustrating the INC MPPT algorithm

Simulation Results for Grid connected system

This simulation illustrates the modelling of a 140 kW grid-connected photovoltaic (PV) plant. The system employs a Perturb and Observe (P&O) Maximum Power Point Tracking (MPPT) algorithm, a traditional Proportional-Integral (PI) controller, and a Proportional-Resonant (PR) controller with harmonic compensator.

The conductance and incremental conductance are swiftly computed and contrasted to ascertain the most advantageous operational state of the module for power generation. Equations offer a succinct depiction of the process.

The subsequent outcomes are obtained from equations (1.1) and (1.2). This algorithm simultaneously measures voltage and current. Hence, changes in the current or voltage indicate the intensity of incoming radiation and the ambient temperature. This technique efficiently monitors the maximum power point (MPP) independent of changes in the environment. This approach alleviates the limitations of the P&O MPPT algorithm in adapting to changing environmental circumstances. During the process of experimental testing, it consistently varies in close proximity to the maximum power point (MPP). The Incremental Conductance (INC) method is more sophisticated than the Perturb and Observe (P&O) MPPT technique. Figure 14 depicts the flowchart, Figure 15 illustrates the flowchart, and Figure 16 showcases the Simulink model of the INC MPPT algorithm.
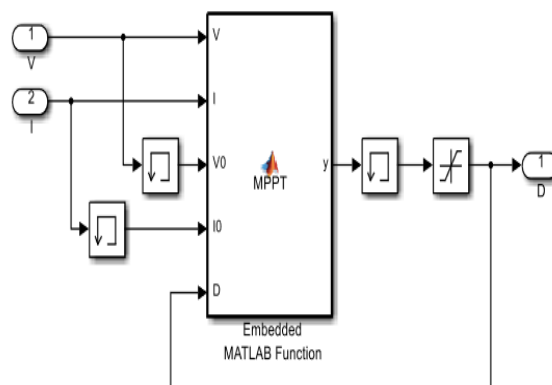

Fig 14. The Simulink model illustrating the Incremental Conductance Maximum Power Point Tracking (INC MPPT) algorithm.
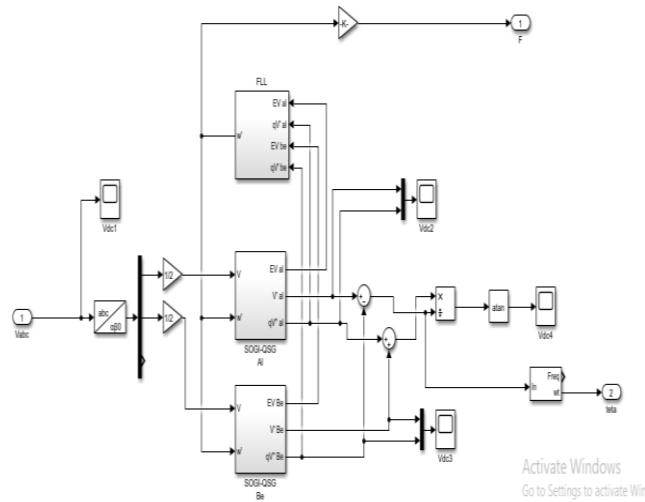
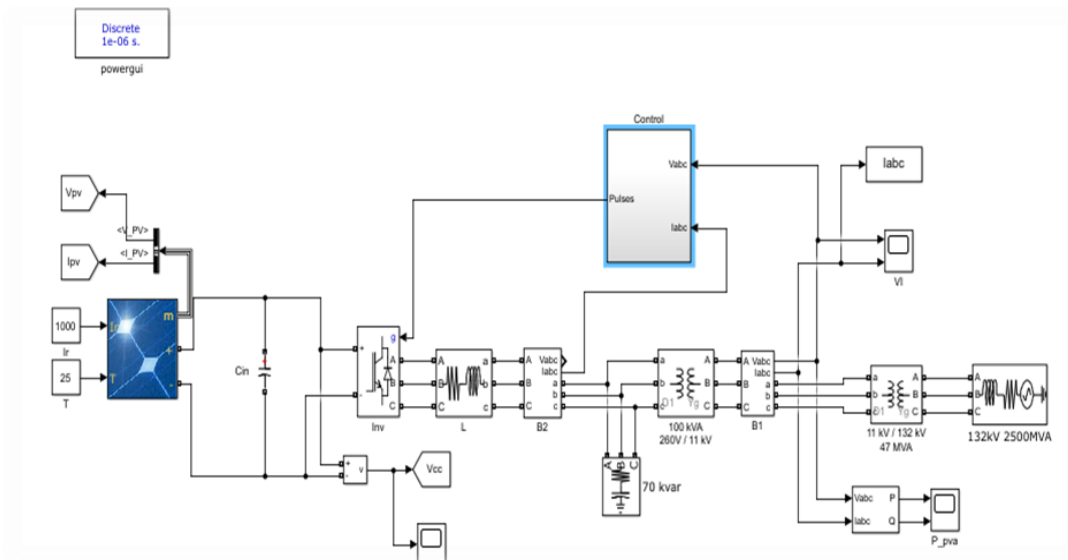**Fig 15.** Simulink model of the DSOGI-FLL synchronisation algorithm.

Fig 16. Simulink model for a photovoltaic (PV) system connected to the electrical grid.
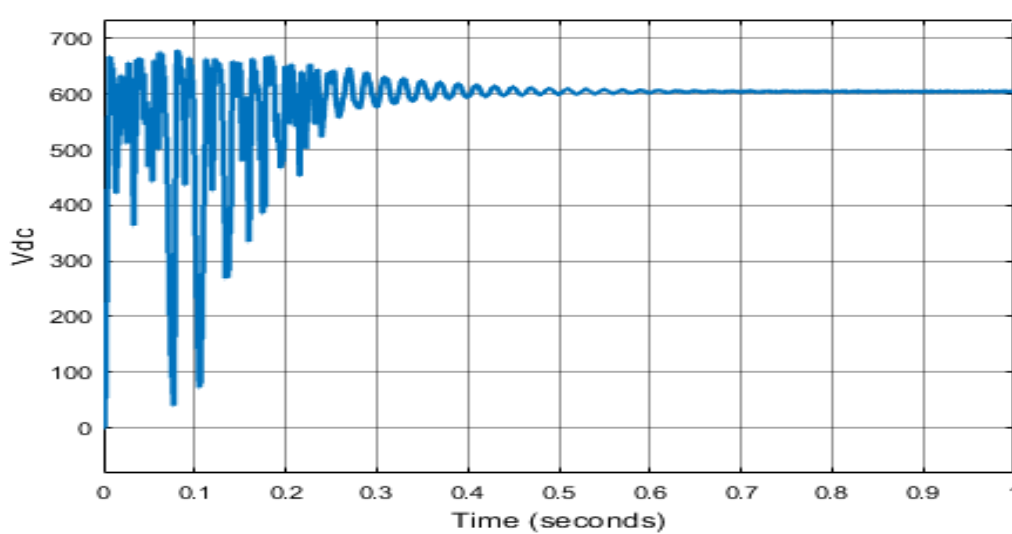

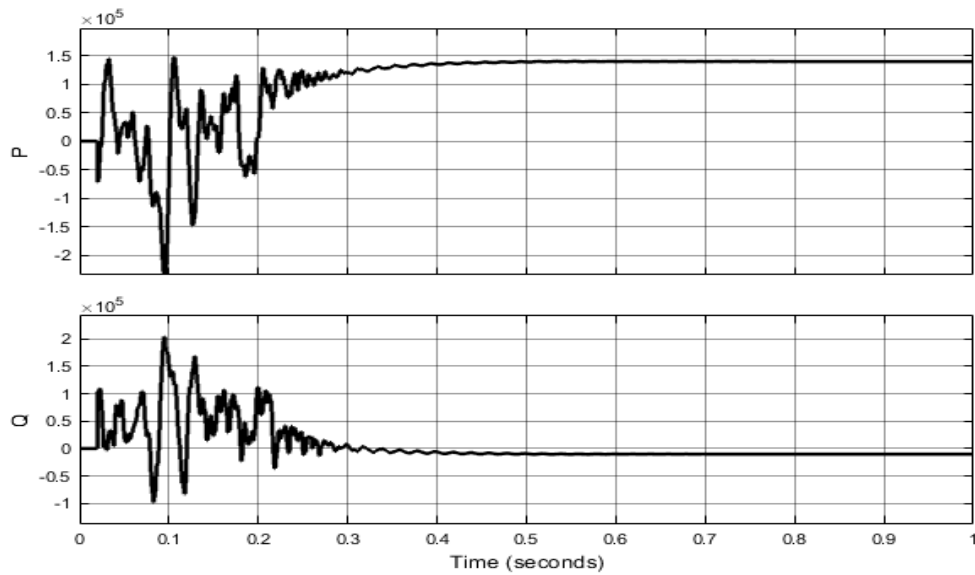**Fig 17.** DC Voltage to the Inverter with PI Controller

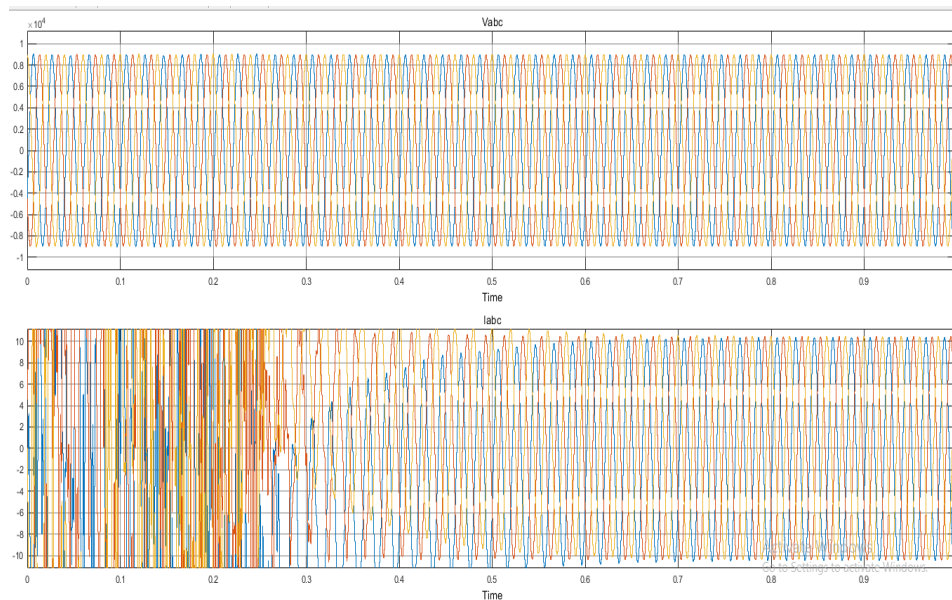**Fig 18.** Real and Reactive Power with PI Controller

Fig 19. Voltage and Current Wave forms with PI Controller

The simulation results are depicted in figures 17, 18, and 19. Evaluating the performance and conduct of the MPP Tracking (MPPT) algorithm and the Photovoltaic (PV) system relies significantly on simulation. In order to achieve this objective, the widely used software Matlab/Simulink has been employed. This software is commonly used for modelling and analysing real-world systems. Computer-based simulations provide a cost-effective and efficient alternative to conducting practical research on SPV systems, considering their complexity and expense.

The whole simulation model of the Solar Photovoltaic (SPV) system, depicted in Figure 20 and Figure 21, comprises the MPPT controller, boost converter, resistive load, and SPV module. Mathematical models are created using Matlab/Simulink to accurately evaluate performance. These models offer valuable insights into how the system behaves in different scenarios. The PV module specifications, which are determined based on the electrical characteristics of a PV module, as well as the boost converter specifications, are detailed in Table 3. By conducting simulations, it is possible to comprehensively analyse and optimise the reaction of the SPV system to the MPPT algorithm.

The Perturb and Observe (P&O) and Incremental Conductance (INC) Maximum Power Point Tracking (MPPT) algorithms inside a Solar Photovoltaic (PV) system were extensively simulated using the Matlab/Simulink software. The simulations were performed using conventional irradiance and temperature settings (G = 1000 W/m2, T = 25°C). Table 4 presents a comparison of the output current,

voltage, and power, highlighting the performance differences between the P&O and INC MPPT algorithms under a resistive load.
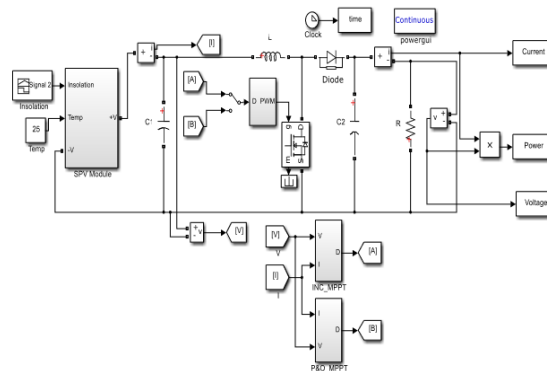

Fig 20. Integrated Solar PV System with MPPT Algorithm for both INC and P&O

Assessing the efficacy of MPPT algorithms involves evaluating efficiency through equation (4.4), with the results tabulated in Table 4.

$$\eta_{MPPT} = \frac{P_m}{P_{max}} * 100\% \qquad (1.15)$$

Here- Pm represents the PV output power derived from simulations and experiments.- max represents the peak power of the Solar Photovoltaic (SPV) module as follows eq'ns (1.15).

(a)

(b)

(c)
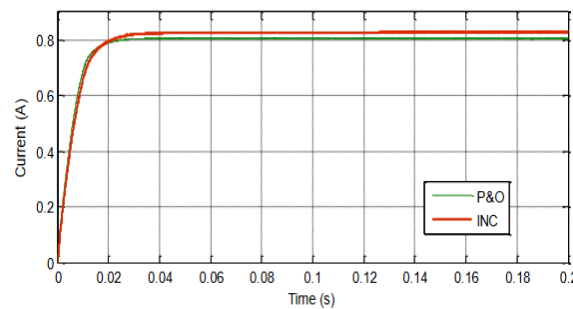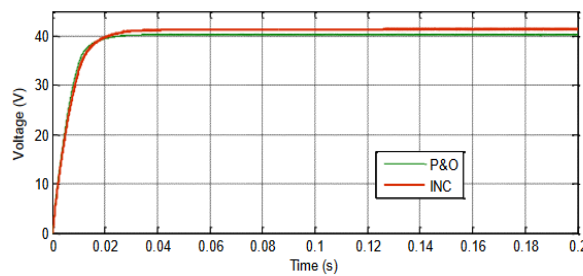
Fig 21. Illustarte the SPV Systems response for equation-based design Under Conditions G=1000W/M2 and T=25 oC (a) Output Current, (b) Output Voltage and (c) Output Power

Table 4. Performance Comparison between P&O and MPPT Algorithm

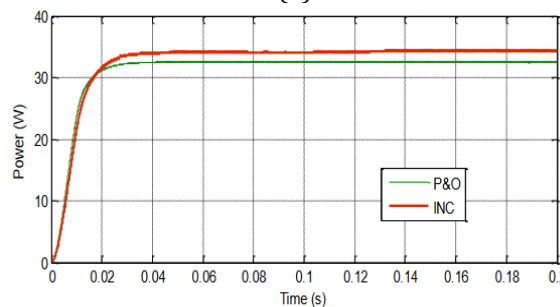| Algorithm	G= 1000 W / m2 , T = 250C		
	Pm	Pmax	Efficiency
P&O	32.58 W	37 W	88.05 %
INC	34.08 W	37 W	92.10 %

From the simulation results, it is evident that INC MPPT algorithm gives better Performance compared to the P&O MPPT algorithm.

CONCLUSION

This study offers a grid-connected Solar Photovoltaic (SPV) system with a maximum power point tracker that is highly effective. Inefficient power transmission occurred when the solar panel was directly connected to the load due to irradiance and fault fluctuations. Maximum power production under varied climatic conditions requires a resilient Maximum Power Point Tracking (MPPT) system. Therefore, an MPPT system is necessary to maximise power production in response to changing air conditions. The Matlab/Simulink-built SPV module, ANFIS controller, and MPPT controller are thoroughly analysed in the research. All modelling methods yielded characteristic curves that matched the manufacturer's datasheet. The I-V and P-V characteristic curves show non-linear SPV module behaviour. This behaviour shows its dependence on irradiation and temperature, emphasising the need for an efficient MPPT system to maximise energy extraction.

Fuzzy algorithms are used to analyse two Maximum Power Point Tracking (MPPT) techniques, Perturb and Observe (P&O) and Incremental Conductance (INC). These solutions were simulated to maximise solar module power.

Different climatic circumstances, sudden load variations, and fault events were used to evaluate conventional Maximum Power Point Tracking (MPPT) methods, such as P&O and INC. System performance was assessed using MATLAB/Simulink.

The study showed that standard Maximum Power Point Tracking (MPPT) approaches cannot accurately detect the MPP under changing weather conditions. This can reduce Solar Photovoltaic (SPV) module performance and system efficiency. To maximise grid-connected photovoltaic (PV) system efficiency, a revised controller was developed. This study improves Solar Photovoltaic (SPV) system efficiency with a Fuzzy Logic MPPT controller. The Fuzzy Logic Controller (FLC) was chosen for complex system control because it does not require a precise mathematical model. Fuzzy logic is a powerful computational approach for solar panel MPP tracking. Nonlinearities and inaccurate data are its specialties. The paper details the architecture of the Fuzzy Logic Controller (FLC), which has two inputs, error (E) and rate of change of error (CE), and one output, the PWM signal duty cycle. The FLC MPPT controller is designed using Matlab/Simulink and tested in different climatic conditions to improve SPV system performance.

The study also created and simulated a Solar Photovoltaic (SPV) module using Matlab/Simulink and three modelling methods. Validation used a Kotak 37 W SPV. Two MPPT algorithms, Incremental Conductance (INC) and Perturb and Observe (P&O), were compared to evaluate the Solar Photovoltaic (SPV) system under constant and changeable environmental conditions. Matlab/Simulink was also used to create and simulate the traditional Maximum Power Point Tracking (MPPT) methods, P&O and INC. Optimising the fuzzy-based controller was suggested to boost system efficiency. Design and simulation of the suggested controller were done in Matlab/Simulink.

Optimising the controller with the Advanced Neuro Fuzzy Inference System was suggested to boost system efficiency. Design and simulation of the suggested controller were done in Matlab/Simulink. Additionally, a photovoltaic (PV) module was constructed and simulated using Matlab/Simulink to assess PV system performance in abnormal conditions. A wind turbine with photovoltaic (PV) technology was built to charge electric cars. The integrated system was simulated in Matlab/Simulink.

REFERENCES
[1]   S. Semsar, Z. Luo, S. Nie and P. W. Lehn, "Integrated Wireless Charging Receiver for Electric Vehicles With Dual Inverter Drives," in IEEE Transactions on Power Electronics, vol. 39, no. 1, pp. 1802-1814, Jan. 2024, doi: 10.1109/TPEL.2023.3320664.

[2]   Y. Zhang, C. Liu, M. Zhou and X. Mao, "A Novel Asymmetrical Quadrupolar Coil for Interoperability of Unipolar, Bipolar, and Quadrupolar Coils in Electric Vehicle Wireless Charging Systems," in IEEE Transactions on Industrial Electronics, vol. 71, no. 4, pp. 4300-4303, April 2024, doi: 10.1109/TIE.2023.3277123.

[3] Z. Hua, K. T. Chau, H. Pang and T. Yang, "Dynamic Wireless Charging for Electric Vehicles With Autonomous Frequency Control," in IEEE Transactions on Magnetics, vol. 59, no. 11, pp. 1-5, Nov. 2023, Art no. 8700405, doi: 10.1109/TMAG.2023.3293793.

[4] O. N. Nezamuddin, C. L. Nicholas and E. C. d. Santos, "The Problem of Electric Vehicle Charging: State-of-the-Art and an Innovative Solution," in IEEE Transactions on Intelligent Transportation Systems, vol. 23, no. 5, pp. 4663-4673, May 2022, doi: 10.1109/TITS.2020.3048728.

[5] A. Mahesh, B. Chokkalingam and L. Mihet-Popa, "Inductive Wireless Power Transfer Charging for Electric Vehicles–A Review," in IEEE Access, vol. 9, pp. 137667-137713, 2021, doi: 10.1109/ACCESS.2021.3116678.

[6] Y. Zhang et al., "Integration of Onboard Charger and Wireless Charging System For Electric Vehicles With Shared Coupler, Compensation, and Rectifier," in IEEE Transactions on Industrial Electronics, vol. 70, no. 7, pp. 7511-7514, July 2023, doi: 10.1109/TIE.2022.3204857.

[7] S. Zhang and J. J. Q. Yu, "Electric Vehicle Dynamic Wireless Charging System: Optimal Placement and Vehicle-to-Grid Scheduling," in IEEE Internet of Things Journal, vol. 9, no. 8, pp. 6047-6057, 15 April15, 2022, doi: 10.1109/JIOT.2021.3109956.

[8] E. Elghanam, M. Ndiaye, M. S. Hassan and A. H. Osman, "Location Selection for Wireless Electric Vehicle Charging Lanes Using an Integrated TOPSIS and Binary Goal Programming Method: A UAE Case Study," in IEEE Access, vol. 11, pp. 94521-94535, 2023, doi: 10.1109/ACCESS.2023.3308524.

[9] B. Mangu, K. K. Kumar and B. G. Fernandes, "A novel grid interactive hybrid power supply system for telecom application," 2011 Annual IEEE India Conference, Hyderabad, India, 2011, pp. 1-5, doi: 10.1109/INDCON.2011.6139543.

[10] J. Rahulkumar. et al., "An Empirical Survey on Wireless Inductive Power Pad and Resonant Magnetic Field Coupling for In-Motion EV Charging System," in IEEE Access, vol. 11, pp. 4660-4693, 2023, doi: 10.1109/ACCESS.2022.3232852.

[11] G. A. Covic, and J. T. Boys, "Inductive power transfer," Proceedings of the IEEE , vol.101, no.6, pp.1276,1289, June 2013.

[12] M. R. R. Razu et al., "Wireless Charging of Electric Vehicle While Driving," in IEEE Access, vol. 9, pp. 157973-157983, 2021, doi: 10.1109/ACCESS.2021.3130099.

[13] D. Patil, M. Ditsworth, J. Pacheco and W. Cai, "A magnetically enhanced wireless power transfer system for compensation of misalignment in mobile charging platforms," IEEE ECCE, 2015, pp. 1286-1293.

[14] Devendra Patil, Marco Sirico, Lei Gu, Babak Fahimi Patil, M. Sirico, L. Gu and B. Fahimi, " Maximum efficiency tracking in wireless power transfer for battery charger: Phase shift and frequency control", Proc. IEEE Energy Conversion Congress and Exposition (ECCE), 18-22 Sept. 2016, Milwaukee, WI, USA.

[15] Vaka Ravikiran, Ritesh Kumar Keshri, Manuele Bertoluzzo, "Efficient Wireless Charging of Batteries With Controlled Temperature and Asymmetrical Coil Coupling" IEEE International Conference on Power Electronics, Drives and Energy Systems (PEDES), Chennai, India, 18-21 Dec. 2018.

[16] Z. Hua, K. T. Chau, H. Pang and T. Yang, "Dynamic Wireless Charging for Electric Vehicles With Autonomous Frequency Control," in IEEE Transactions on Magnetics, vol. 59, no. 11, pp. 1-5, Nov. 2023, Art no. 8700405, doi: 10.1109/TMAG.2023.3293793.

[17] Ravi Bukya, Mangu, A. Jayaprakash and Jatoth Ramesh " A Study on Current-fed Topology for Wireless Resonant Inductive Power Transfer Battery Charging System of Electric Vehicle" PARC-2020, feb-28-29, vol.1, pp May-2020.

[18] Y. Zhang, S. Chen, X. Li, Z. She, F. Zhang and Y. Tang, "Coil Comparison and Downscaling Principles of Inductive Wireless Power Transfer Systems," 2020 IEEE PELS Workshop on Emerging Technologies: Wireless Power Transfer (WoW), Seoul, Korea (South), 2020, pp. 116-122, doi: 10.1109/WoW47795.2020.9291295.

[19] H. Wang, U. Pratik, A. Jovicic, N. Hasan and Z. Pantic, "Dynamic Wireless Charging of Medium Power and Speed Electric Vehicles," in IEEE Transactions on Vehicular Technology, vol. 70, no. 12, pp. 12552-12566, Dec. 2021, doi: 10.1109/TVT.2021.3122366.

[20] Y. Li et al., "A New Magnetic Coupler with High Rotational Misalignment Tolerance for Unmanned Aerial Vehicles Wireless Charging," in IEEE Transactions on Power Electronics, vol. 37, no. 11, pp. 12986-12991, Nov. 2022, doi: 10.1109/TPEL.2022.3184335.

[21] R. Bukya, B. Mangu, B. Bhaskar and B. Bhavsingh, "Analysis of Interoperability Different Compensation Network in Wireless EV Charging Systems," 2021 2nd Global Conference for Advancement in Technology (GCAT), Bangalore, India, 2021, pp. 1-6, doi: 10.1109/GCAT52182.2021.9587618.

[22] D. Kishan, M. Vinod and N. Harishchandra, "Magnetic Coupling Characteristics of Spiral Square - Circular Coupled Coils for Wireless EV Battery Charging System," 2020 IEEE 17th India Council International Conference (INDICON), New Delhi, India, 2020, pp. 1-5, doi: 10.1109/INDICON49873.2020.9342265.

[23] Y. Yao, S. Gao, J. Mai, X. Liu, X. Zhang and D. Xu, "A Novel Misalignment Tolerant Magnetic Coupler for Electric Vehicle Wireless Charging," in IEEE Journal of Emerging and Selected Topics in Industrial Electronics, vol. 3, no. 2, pp. 219-229, April 2022, doi: 10.1109/JESTIE.2021.3051550.

[24] Y. Yorozu, M. Hirano, K. Oka, and Y. Tagawa, "Electron spectroscopy studies on magneto-optical media and plastic substrate interfaces (Translation Journals style)," IEEE Transl. J. Magn.Jpn., vol. 2, Aug. 1987, pp. 740–741 [Dig. 9th Annu. Conf. Magnetics Japan, 1982, p. 301.

[25] R. Bukya, B. Mangu, B. Bhaskar and J. Ramesh, "Design and Performance Analysis of Compensation Capacitors In P-S Topology for Wireless System on Receiver Side," 2022 IEEE 2nd International Conference on Sustainable Energy and Future Electric Transportation (SeFeT), Hyderabad, India, 2022, pp. 1-6, doi: 10.1109/SeFeT55524.2022.9909354.

[26] K. Aditya; S. Williamson, "A Review of Optimal Conditions for Achieving Maximum Power Output and Maximum Efficiency for a Series-Series Resonant Inductive Link," in IEEE Transactions on Transportation Electrification, vol. no.99, pp.1-1

[27] B. Mangu and B. G. Fernandes, "Multi-Input Transformer Coupled DC-DC converter for PV-Wind based Stand-Alone Single Phase Power Generating System," IEEE Energy Conversion Congress and Exposition, ECCE'2014, Pittsburgh, Pennsylvania, USA, Sept. 2014.

[28] S. Samanta, A. K. Rathore and S. K. Sahoo, "Current-fed full-bridge and half-bridge topologies with CCL transmitter and LC receiver tanks for wireless inductive power transfer application," 2016 IEEE Region 10 Conference (TENCON), Singapore, 2016, pp. 756-761, doi: 10.1109/TENCON.2016.7848105.

[29] V. B. Pamshetti et al., "Cooperative Operational Planning Model for Distributed Energy Resources With Soft Open Point in Active Distribution Network," in IEEE Transactions on Industry Applications, vol. 59, no. 2, pp. 2140-2151, March-April 2023, doi: 10.1109/TIA.2022.3223339.

[30] V. Balu, K. Krishnaveni and P. Srinivas, "TSK-Fuzzy Controllers for Novel Energy Management System of Renewable Energy Sources based AC Microgrid with Five Level Inverter," 2022 IEEE 10th Power India International Conference (PIICON), New Delhi, India, 2022, pp. 1-6, doi: 10.1109/PIICON56320.2022.10045092.

[31] M. Vinod, D. Kishan and B. D. Reddy, "Three-Leg DC–DC Converter for Efficient Inductive Power Transfer of Electric Vehicles for Wide-Range Battery Applications," in IEEE Transactions on Power Electronics, vol. 38, no. 8, pp. 9317-9321, Aug. 2023, doi: 10.1109/TPEL.2023.3269886.

[32] B. V. Vani, D. Kishan, M. W. Ahmad, S. Hanumanthakari and B. N. K. Reddy, "A Technological Research on Electric Vehicles Charging Approaches and Optimization Methods," 2022 IEEE 12th Symposium on Computer Applications & Industrial Electronics (ISCAIE), Penang, Malaysia, 2022, pp. 191-195, doi: 10.1109/ISCAIE54458.2022.9794511.

[33] M. Mohammad, O. C. Onar, V. P. Galigekere, G. -J. Su and J. Wilkins, "Magnetic Shield Design for the Double-D Coil-Based Wireless Charging System," in IEEE Transactions on Power Electronics, vol. 37, no. 12, pp. 15740-15752, Dec. 2022, doi: 10.1109/TPEL.2022.3191911.

[34] S. Anand, R. S. Farswan, B. Mangu and B. G. Fernandes, "Optimal charging of battery using solar pv in standalone dc system," 6th IET International Conference on Power Electronics, Machines and Drives (PEMD 2012), Bristol, 2012, pp. 1-6, doi: 10.1049/cp.2012.0339.

[35] Pradipta Patra, Susovon Samanta, Amit Patra, Souvik Chattopadhyay, "A Novel Control Technique for Single-Inductor Multiple-Output DC-DC Buck Converters", IEEE International Conference on Industrial Technology, Mumbai, India, 15-17 Dec. 2006.

[36] Suvendu Samanta, Akshay Kumar Rathore, Sanjib Kumar Sahoo, "Current-fed full-bridge and half-bridge topologies with CCL transmitter and LC receiver tanks for wireless inductive power transfer application", IEEE Region 10 Conference (TENCON), Singapore, 22-25 Nov. 2016.

[37] A. Kurs, A. Karalis, R. Moffatt, J. D. Joannopoulos, P. Fisher, and M. Soljacic, "Wireless power transfer via strongly coupled magnetic resonances," Science, Vol. 317, 83-86, 2007.